JOURNAL OF THE ROYAL SOCIETY Interface

Effects of surface microtopography on the assembly of the osteoclast resorption apparatus

Dafna Geblinger, Christian Zink, Nicholas D. Spencer, Lia Addadi and Benjamin Geiger

J. R. Soc. Interface 2012 **9**, 1599-1608 first published online 16 November 2011
doi: 10.1098/rsif.2011.0659

JOURNAL OF THE ROYAL SOCIETY Interface

J. R. Soc. Interface (2012) **9**, 1599–1608
doi:10.1098/rsif.2011.0659
Published online 16 November 2011

Effects of surface microtopography on the assembly of the osteoclast resorption apparatus

Dafna Geblinger[1,2], Christian Zink[3], Nicholas D. Spencer[3], Lia Addadi[2] and Benjamin Geiger[1,*]

[1]*Department of Molecular Cell Biology, and* [2]*Department of Structural Biology, Weizmann Institute of Science, Rehovot 76100, Israel*
[3]*Laboratory for Surface Science and Technology, Department of Materials, ETH Zurich, Wolfgang-Pauli-Strasse 10, 8093 Zürich, Switzerland*

Bone degradation by osteoclasts depends on the formation of a sealing zone, composed of an interlinked network of podosomes, which delimits the degradation lacuna into which osteoclasts secrete acid and proteolytic enzymes. For resorption to occur, the sealing zone must be coherent and stable for extended periods of time. Using titanium roughness gradients ranging from 1 to 4.5 μm R_a as substrates for osteoclast adhesion, we show that microtopographic obstacles of a length scale well beyond the range of the 'footprint' of an individual podosome can slow down sealing-zone expansion. A clear inverse correlation was found between ring stability, structural integrity and sealing-zone translocation rate. Direct live-cell microscopy indicated that the expansion of the sealing zone is locally arrested by steep, three-dimensional 'ridge-like barriers', running parallel to its perimeter. It was, however, also evident that the sealing zone can bypass such obstacles, if pulled by neighbouring regions, extending through flanking, obstacle-free areas. We propose that sealing-zone dynamics, while being locally regulated by surface roughness, are globally integrated via the associated actin cytoskeleton. The effect of substrate roughness on osteoclast behaviour is significant in relation to osteoclast function under physiological and pathological conditions, and may constitute an important consideration in the design of advanced bone replacements.

Keywords: osteoclast; bone remodelling; cytoskeleton; biocompatible materials; roughness

1. INTRODUCTION

Bone growth and remodelling are tightly regulated by the balanced activities of osteoclasts and osteoblasts, whose functions are bone resorption and new bone formation, respectively. An imbalance between the activities of these two cell types leads to pathological conditions such as osteoporosis, caused by excessive osteoclast activity, and osteopetrosis, caused by reduced osteoclast activity [1]. Furthermore, bone resorption around implants [2,3] is a major cause of failure of orthopaedic and dental implants, leading to implant loosening and micromotion problems. Understanding which cues trigger or arrest bone remodelling is thus important for the design of implants that improve osseointegration.

Osteoclasts are multi-nucleated cells of monocytic origin, which alternate between migratory and bone-resorbing phases [4]. Their attachment to the bone surface is mediated through unique adhesion structures, the podosomes, which consist of a central core of actin filaments linked via lateral fibres to a membrane-bound, circular adhesion plaque surrounding the core [5]. The actin filaments are associated with a variety of proteins that regulate their nucleation, elongation, severing and bundling [6,7], whereas the membrane anchorage is mediated via components of the integrin adhesome [8–11]. In the functional, polarized, bone-resorbing osteoclast, podosomes assemble into a ring-like superstructure, known as a 'sealing zone' [5,12]. This structure mediates the firm attachment of the cell to the substrate, delimiting the so-called 'resorption lacuna' at the bone surface, and thus serving as a diffusion barrier that separates the resorption area from the rest of the extracellular environment. The sealing zone formed on the bone, and on a variety of artificial adhesion surfaces, is composed of a central F-actin ring, formed of a network of interlinked podosomes, and flanked by inner and outer rings of integrins and associated adhesome proteins [5,12].

A key requirement for bone degradation is that the resorption lacuna must be well-defined and isolated, and thus the sealing zone should be continuous and sufficiently stable over time to allow resorption to occur. This requirement is not trivial when considering that the sealing zone is a very dynamic structure [13,14], whose continuity depends on multiple environmental factors, including but not limited to surface chemistry, degree of mineralization, substrate rigidity and surface

*Author for correspondence (benny.geiger@weizmann.ac.il).

Electronic supplementary material is available at http://dx.doi.org/10.1098/rsif.2011.0659 or via http://rsif.royalsocietypublishing.org.

Received 27 September 2011
Accepted 24 October 2011

topography [15–19]. We have previously shown that sealing-zone structure and dynamics depend on the nature of the underlying matrix, and are vastly different for cells adhering to calcite, glass or bone [18]. We have further demonstrated that osteoclast adhesion to bone is spatially selective, insofar as there are bone regions that locally induce sealing-zone formation, while other regions, under the same cell and at the same time, fail to do so.

We have further shown that one of the features that effectively modulates sealing-zone formation is the submicrometre surface roughness. As our primary model substrate, we have used 'smooth' and 'rough' calcite crystals, demonstrating that the level of substrate roughness has a profound effect on the formation and stability of the sealing zone, and the associated F-actin ring [19]. Thus, smooth surfaces (average roughness $R_a \sim 12$ nm) induced the formation of small and unstable actin rings, while sealing zones formed on rough calcite surfaces (average roughness $R_a > 0.5$ μm) are considerably larger and more stable. It was further observed that steps or submicrometre cracks on a smooth surface stimulate local ring formation, raising the possibility that imperfections on bone surfaces may induce local resorptive activity.

While the evidence concerning the ability of osteoclasts to sense and respond to surface roughness is compelling, there are many open questions concerning the nature of the sensory mechanism. Although the subject of nanotopography sensing by cells is extensively studied and discussed [20–29], the possible effect of cooperativity in topography sensing within the range of several micrometres has not been addressed. Issues that must still be clarified include the dimensions and angles of the topographical features that are sensed by the cells and whether the topography-sensing mechanism acts at the level of the individual podosome, or of the entire sealing zone.

To address these questions, we have used here surfaces with a gradient of roughness values and have monitored the effect of the local topography on osteoclast behaviour and sealing-zone dynamics. We show here that sealing-zone dynamics are affected by changes in topography at a scale larger than that of a 'footprint' of a single podosome, implying that surface-topography sensing, at this scale, is most probably integrated by the sealing zone. We show that the expansion of the sealing zone is arrested by steep, three-dimensional 'ridge-like barriers', running parallel to its perimeter. Nevertheless, the arrested region can overcome such obstacles and move across them, when flanking regions of the sealing zone expand through neighbouring, obstacle-free areas, apparently 'towing' the arrested region. When steep slopes restrict the expansion of the ring in all directions, the sealing zone adapts to the surrounding topography and becomes stable and continuous. We conclude that the three-dimensionality of the underlying surface globally affects sealing-zone assembly, dynamics and stability.

2. MATERIAL AND METHODS

2.1. Surface preparation

Gradient surfaces were prepared as previously described. In short, the gradients were prepared by sandblasting aluminium surfaces, followed by their immersion in a polishing solution. The surfaces were then gradually removed from the solution such that a gradient was formed owing to the varying duration of the polishing process for different locations on the surface. To reproduce identical surfaces, the aluminium surface was then used as a template for preparing replica surfaces made of epoxy resin (via an elastomeric intermediate), which were then sputtered with 60 nm of titanium [25].

The gradients were characterized with an optical profilometer (Plu NEOX, Sensofar, Spain) by using the 50X objective (NA 0.95) in confocal mode. For every data point, several measurements were performed on a 2.5 mm-long stripe perpendicular to the gradient. The data were analysed with the Software SensoMap (v. 6.0.0.5832 incl. 3D Fourier Analysis Module, DigitalSurf, France) by levelling the measurements and extracting 10 profiles, each 20 pixels apart. The profiles were then split into different roughness windows (1.5–3 μm, 3–10 μm, 10–50 μm, 50–250 μm) by using the fast Fourier transform (FFT) filter module. For every roughness window, the corresponding R_a value was calculated according to the ASME B46.1 standard without applying any additional filtering. Then, the average roughness and the standard deviation of the 10 profiles were calculated.

Surfaces were plasma-cleaned for 2 min, immersed in 70 per cent ethanol for 10 min and conditioned with vitronectin (10 μg ml^{-1}) for 8–10 h at 4°C. Prior to cell plating, the gradient surfaces were washed, placed in the culture medium and heated to 37°C.

2.2. Tissue culture

RAW 264.7 cells, a mouse leukemic, monocyte-macrophage cell line, obtained from the American Type Culture Collection (ATCC; Manassas, VA, USA) were cultured at 37°C in a 5 per cent CO_2-humidified atmosphere in Dulbecco's modified Eagle's medium with Earle's salts, L-glutamine and $NaHCO_3$, supplemented with foetal bovine serum and antibiotics. To induce osteoclast differentiation, cells were plated at a density of 100 cells mm^{-2} in alpha-minimal essential medium supplemented with soluble receptor activator of the NFκB ligand (RANK-L; 20 ng ml^{-1}), and macrophage colony-stimulating factor (M-CSF; 20 ng ml^{-1}). After 3 days, cells were removed with ethylene diaminetetraacetic acid (10 mM) for 10 min, and then cultured for 60 h on the microgradient surfaces.

2.3. Fluorescence microscopy

For live-cell imaging, RAW cells stably expressing GFP (green fluorescent protein)-actin [30] were induced to differentiate in plastic dishes for 3 days, then suspended and replated on gradient surfaces as described above, and observed for 48 h in sequential periods of 8–12 h, starting 4 h after replating. The temporal resolution recorded is 1 frame min^{-1}. Images were acquired using a DeltaVision microscopy system (Applied Precision, Inc., Issaquah, WA, USA) consisting of an IX70 inverted microscope equipped with a 20X/0.7 objective (Olympus, Japan).

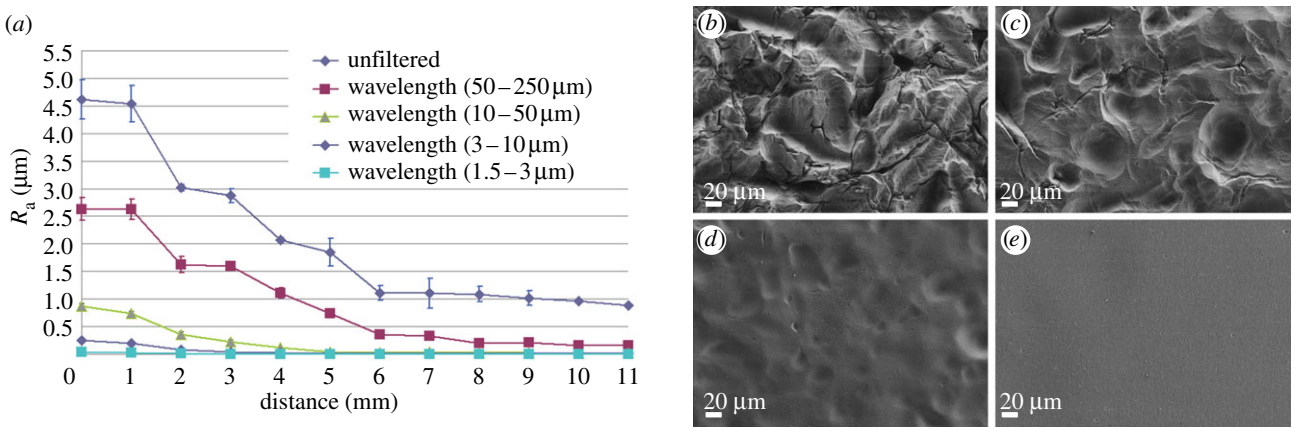

Figure 1. Characterization of the gradient surface. (*a*) Average R_a values along the gradient and its decomposition into components of different length scale (wavelength). (*b–e*) SEM micrographs of selected locations along the gradient. (*b*) Sandblasted area that did not undergo smoothing: note the abundance of sharp edges, ridges and peaks, $R_a = 4.6$ µm (unfiltered); (*c*) 2 mm into the gradient, $R_a = 3$ µm (unfiltered): note that the edges are rounded; (*d*) 5 mm into the gradient, $R_a = 1.9$ µm (unfiltered); (*e*) the smoothest part of the gradient, $R_a = 0.9$ µm (unfiltered).

Image processing and analysis were carried out using PRISM software for LINUX operating systems (http://msg.ucsf.edu/IVE/Download/).

For acquisition of the three-dimensional structure of the sealing zone, GFP-actin-expressing osteoclasts were fixed and stained with a primary antibody, monoclonal anti-paxillin (BD, San Jose, CA, USA), and a secondary antibody, goat anti-mouse IgG, conjugated to cy3 (Jackson ImmunoResearch Laboratories, Inc., West Grove, PA, USA), following well-established procedures [5].

In order to plot the correlation graph, we first averaged the fraction of identical pixels in subsequent frames of a 150 min movie between frames separated by $\Delta t = 0–15$ min. This resulted in a correlation graph per cell. We then averaged the correlation graphs obtained for several cells (see n values in figure 6) for each topographical zone (defined above; figure 3). As the stability of the sealing-zone structure increases, the decay in correlation becomes slower.

The kymograph was plotted using IMAGEJ. In short, for each frame of a time series, grey values along a line of interest are read out. From these lines of grey values, a new image (time-space plot) is assembled: The line read from the first frame of the time series is put down as the first line in the kymograph, the line from the second frame as the second line of the kymograph, and so forth. In this way, the x-axis of the kymograph becomes a time axis and the unit is the time-interval of the sequence (1 min). The y-axis is the distance along the line.

3. RESULTS

3.1. Surface characterization

Roughness gradients were produced by first sandblasting an aluminium surface, then dipping it into a polishing solution and gradually retracting it, as has been previously described [25]. The aluminium gradients so obtained through the combined roughening effect of sandblasting and the progressive smoothing effect of the polishing solution, then served as templates for the production, via an elastomeric intermediate, of a large number of identical epoxy roughness replicas, which were subsequently coated with titanium [25]. The procedure resulted in gradients distributed over an overall length of 10 mm within an average roughness range of 0.4–4.5 µm R_a (figure 1*a*). Average roughness (R_a) is defined as the average displacement of measured points relative to the mean plane. FFT was applied to convert the roughness measurements acquired along the gradient into power spectra that could then be Fourier-filtered into roughness profiles corresponding to different wavelength (length-scale) windows [31] of 1.5–3 µm, 3–10 µm, 10–50 µm and 50–250 µm. Figure 1 shows the decay of the roughness/amplitude values for each range of wavelengths as a function of the position along the gradient. Scanning electron microscopy images were also taken at different positions on the gradient, corresponding to different polishing times. Where the surface was not polished, sharp edges, ridges and peaks created by the sandblasting procedure can be observed (figure 1*b*). The gradual polishing resulted in increasing smoothing of these features, rendering them shallower and larger in diameter (figure 1*b–e*).

The local features of the gradient substrate were characterized by monochromatic reflected-light microscopy, in which light intensity is locally correlated with the angle between the surface plane and the incident light. In order to distinguish between peaks and pits, we examined the surface at different Z-planes. The two images shown in figure 2*a*,*b* are taken at two focal planes, 8.5 µm apart, in a zone with $R_a \sim 4$ µm (unfiltered): the different features that are in focus in each focal plane demonstrate that the rounded feature in the image is an approximately 8.5 µm-deep pit. The features from reflected-light images can be subsequently reconstructed according to the brightness of the reflected image (figure 2*c*,*d*). This characterization was performed *in situ* while monitoring dynamics of fluorescently tagged actin within the cells, enabling us to establish a direct correlation between the underlying substrate topography and the sealing-zone dynamics.

In order to facilitate the establishment of a correlation between the behaviour of cell populations at different

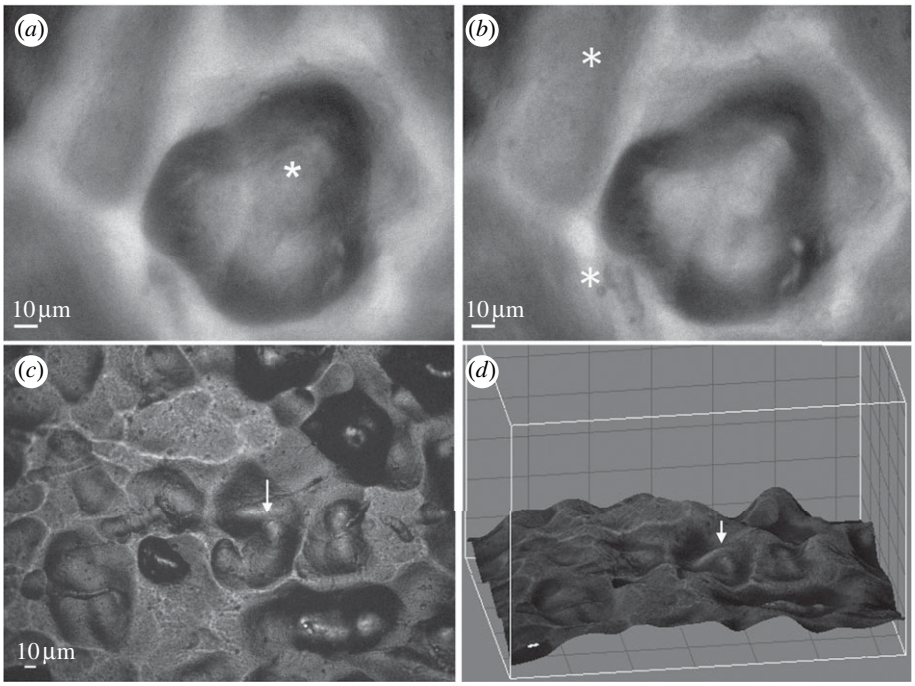

Figure 2. Three-dimensional representation of the topographical surface. (*a*,*b*) Images of the surface, viewed by reflection microscopy, at two focal planes, 8.5 µm apart. In (*a*), the focus is on the bottom of the rounded pit; in (*b*), the focus is on the surrounding 'rim'. The areas focused on are marked with asterisks. (*c*) Reflection image of a surface, (*d*) represented in three dimensions. For easier reference, the same spot is marked with arrows in (*c*) and in (*d*).

positions and the surface roughness, we divided the gradient into five different zones according to their local topographical features (figure 3), as follows: zone 1: relatively smooth surface ($R_a < 0.7$ µm, unfiltered); zone 2: scattered shallow pits, mostly separated by smooth areas (0.7 µm $> R_a >$ 1.5 µm, unfiltered); zone 3: deeper pits separated by rounded ridges (1.5 µm $< R_a <$ 3 µm, unfiltered); zone 4: multiple, overlapping round deep pits (3 µm $< R_a <$ 4 µm, unfiltered); zone 5: sand-blasted surface which was not polished and hence is mainly dominated by sharp edges ($R_a \sim 4$ µm, unfiltered). In general, as the average roughness (R_a) increases and the distance between profile irregularities decreases, the angles in the area are steeper. The decay in the roughness of different wavelength components of the roughness profile (figure 1*a*) is reported in figure 3 in relation to the different zones.

All gradient replicas used in this study originated from the same, extensively characterized original template, ensuring that all surfaces used in different experiments are identical and the cells tested in different experiments thus encounter identical topography.

3.2. Sealing-zone dynamics

RAW 264.7 cells, expressing GFP-actin, were induced to differentiate by 3-day exposure to RANK ligand and M-CSF. The mature osteoclasts were removed from the plate and seeded on the roughness-gradient surfaces. Several cells located at different positions along the gradient were monitored simultaneously over 12 h. In order to determine whether the osteoclast sealing-zone geometry is affected by substrate topography, we acquired a focal series of sealing-zone images of cells expressing GFP-tagged actin and immunolabelled for paxillin, and subjected the images to three-dimensional deconvolution. As shown in figure 4, the sealing-zone ring acquires the three-dimensionality of the surface. In areas with smaller R_a (zone 1: $R_a \sim 0.5$ µm, unfiltered), the rings appear to be largely flat, whereas in areas with high roughness (zone 5: $R_a \sim 4$ µm, unfiltered), both the actin and the paxillin rings are clearly three-dimensional, most probably guided by the topography of the surface. The paxillin staining appears to be more closely associated with the surface, relative to actin, as might be expected when considering that the adhesion plaque, including paxillin, is tightly associated with the ventral cell membrane. It appears that the shape of the ring is at least partially dictated by the sharp edges of the surface. Furthermore, while on the relatively smooth surfaces, the sealing zone is mostly circular, as the roughness increases, deviations from a circular shape become more pronounced (figure 4).

Observation of a large number of fixed cells along the gradient showed an increasing integrity of the sealing zone, with increasing roughness. The percentage of fragmented rings with a gap of at least 10 µm decreased from zones 1 to 5, as R_a increased (figure 5). This finding clearly demonstrates that as the surface is more three-dimensional and the expanding rings encounter more obstacles, the integrity of the ring is better preserved, while on a flatter surface where the expanding ring encounters no obstacles, the integrity of the ring is compromised.

Osteoclasts on the titanium gradient form large rings that spread towards the periphery of the cell. In order to assess the stability of the sealing-zone rings formed by cells adhering to the various zones, we calculated the fraction of identical pixels in subsequent frames of a movie. A fraction closer to 1 indicates that the main features in the pictures (the sealing-zone ring) remained in

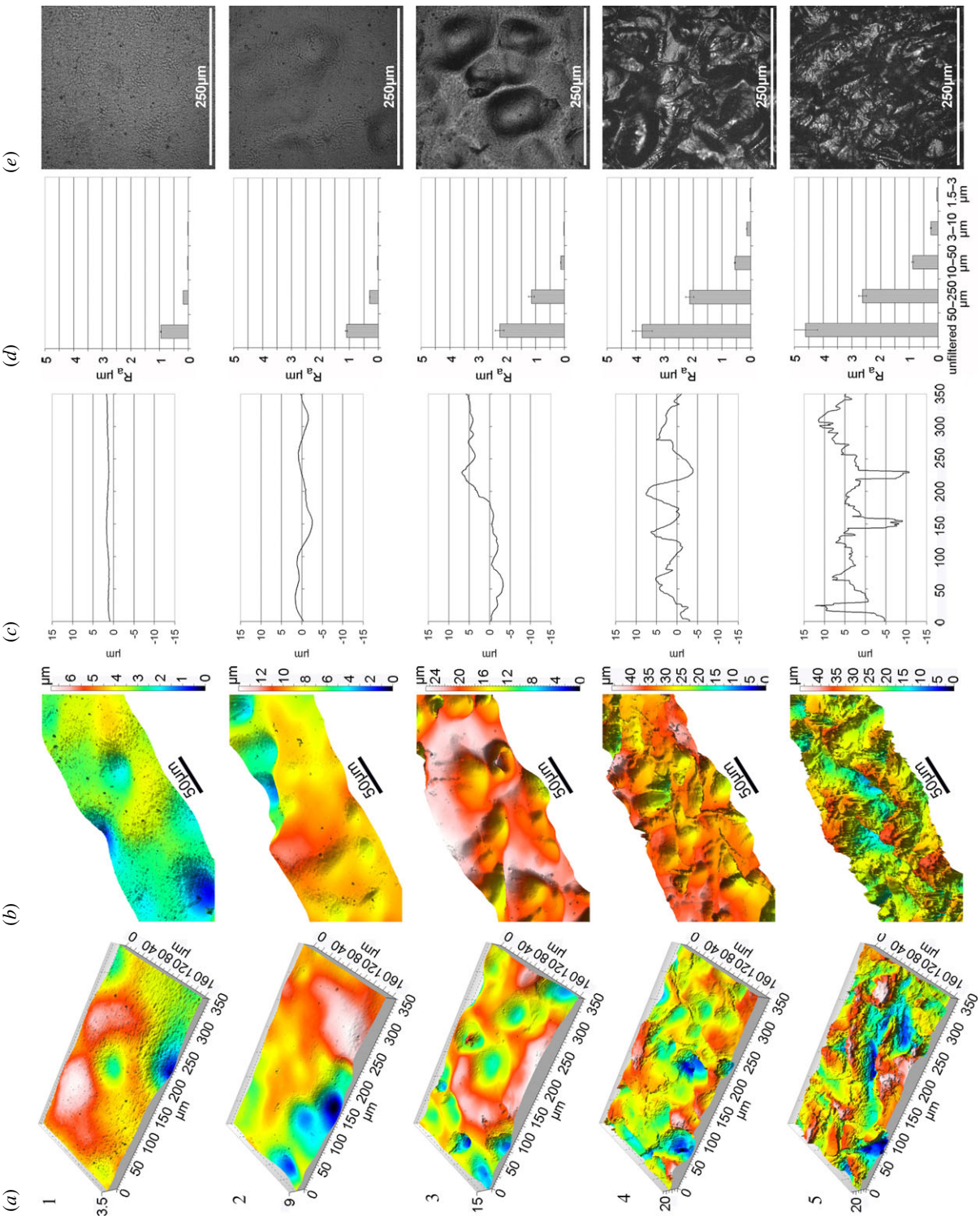

Figure 3. Topography of the surface divided into zones 1–5. (*a*,*b*) Three-dimensional image of the sample from different angles. The colour code represents heights from blue (low) to white (high). Note that the colour scale is different for every zone. (*c*) Line profile taken in an arbitrary position within the zone. For comparison, all zones were drawn to the same 30 µm scale. (*d*) The R_a values for different wavelength windows. (*e*) Light reflection images of the different zones.

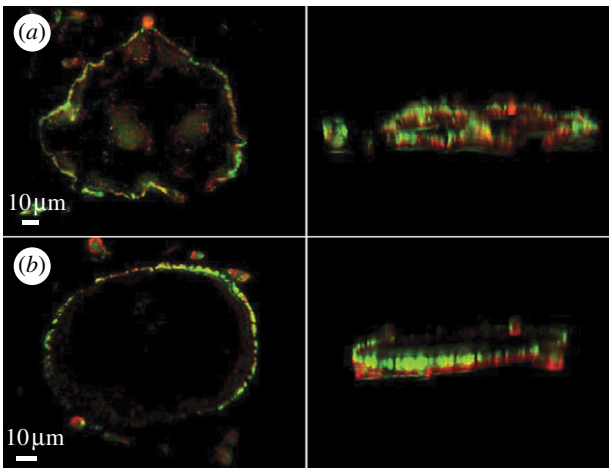

Figure 4. Three-dimensional deconvolution of sealing-zone ring images on a surface with (*a*) $R_a \sim 4\,\mu m$ (unfiltered) and (*b*) $R_a \sim 0.5\mu m$ (unfiltered). Note that the sealing zone on the rough surface acquires the topography of the surface.

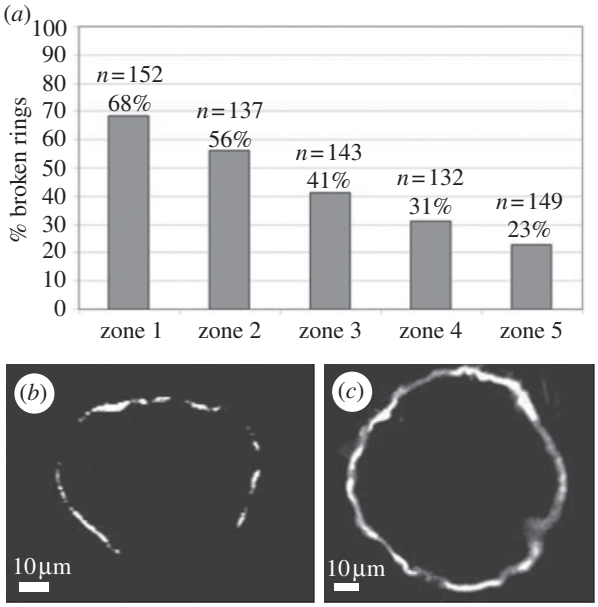

Figure 5. Monitoring of the percentage of fragmented rings with gaps of at least 10 μm. (*a*) Histograms showing that from zones 1 to 5, as R_a increases, the rings are more continuous. (*b*) A characteristic image of a fragmented sealing-zone ring on zone 1 ($R_a < 0.7\,\mu m$, unfiltered). (*c*) Continuous sealing-zone ring on zone 5 ($R_a \sim 4\mu m$, unfiltered).

the same position. The correlation between frames separated by $\Delta t = 0$–15 min was averaged for all frames in a movie of 150 min. We then averaged the correlation calculated for several cells (see n values in figure 6) for every topographical zone (defined above; figure 3). The sealing-zone rings in zones 1–3 are somewhat unstable, as reflected by the relatively low correlation values, but their stability increases substantially in zones 4 and 5, with increasing roughness. Interestingly, the sealing-zone stability of cells on zone 5 ($R_a \sim 4\,\mu m$) and zone 4 ($3\,\mu m < R_a < 4\,\mu m$) is clearly different, although they are relatively close in their unfiltered roughness values and mainly differ by the sharpness of the edges (figure 4). This implies that the ring dynamics are not simply directly proportional to the average roughness of the sample. Examining the composition of the roughness of zones 4 and 5 in terms of different wavelength windows shows that the relevant range for the sealing-zone stability is either $R_a = 0.5$–$1\,\mu m$ for $\lambda = 10$–$50\,\mu m$ or even as low as 0.1–0.3 μm for $\lambda = 3$–$10\,\mu m$. In both cases, the wavelength is larger than the size of a podosome, indicating that sensing of the substrate roughness occurs not at the scale of individual podosomes, but of a number of podosomes linked together in the sealing zone.

As the sealing zone closely adapts to the surface topography (figure 4), it is evident from the above data that extracellular microtopographic obstacles affect sealing-zone formation and turnover. This effect appears to be mostly local, as we have observed that different regions of the same sealing zone, encountering or not encountering a topographical barrier, can be arrested or continue to expand. In this case, it is interesting to explore the long-range mechanical constraints of the sealing-zone ring, i.e. the dynamic correlation between 'arrested regions' and adjacent 'free regions'.

To address this issue, we have examined the local and global dynamic properties of the sealing zone in osteoclasts plated on zone 3 in which pits and peaks are separated by short smooth areas ($1.5\,\mu m < R_a < 3\,\mu m$, unfiltered). Electronic supplementary material, movie S1, from which the pictures shown in figure 7*a* and the kymographs in figure 7*c*,*d*,*e* were taken (see §2) show that the progression of the sealing-zone region encountering a topographic barrier (*d*) is stalled relative to its surroundings (*c* and *e*), yet once the flanking regions have advanced beyond the barrier, the stalled region of the ring is 'pulled over' the barrier and lines up with the rest of the sealing zone.

4. DISCUSSION

The primary objective of this study was to elucidate the effect of surface microtopography on sealing-zone structure and dynamics in cultured osteoclasts. We show here that sealing-zone stability and integrity are increased, and translocation of the sealing zone decreased, with increased surface roughness. These results further indicate that the sealing-zone translocation rate is inversely correlated to its integrity.

The sealing zone is built of individual podosomes, each consisting of a core of actin bundles that rise perpendicular to the surface, surrounded by actin fibres connecting the core to the membrane. In the sealing zone, the podosomes are interconnected by a dense network of actin fibres joining one core to the other and to the substrate. The typical dimensions of a single isolated podosome are approximately 1 μm in diameter and up to 4 μm high [5,32]. In the sealing-zone ring on glass, interconnected podosomes are separated by a typical core-to-core distance of approximately 500 nm. Our finding that the capability of osteoclasts to detect and react to increasing surface topographies is expressed at wavelengths larger than 3 μm, within a range well beyond the size of individual podosomes, renders unlikely the possibility that topography sensing is carried out by single podosomes and suggests that topography sensing is dependent upon the cooperation of podosomes in the sealing-zone network.

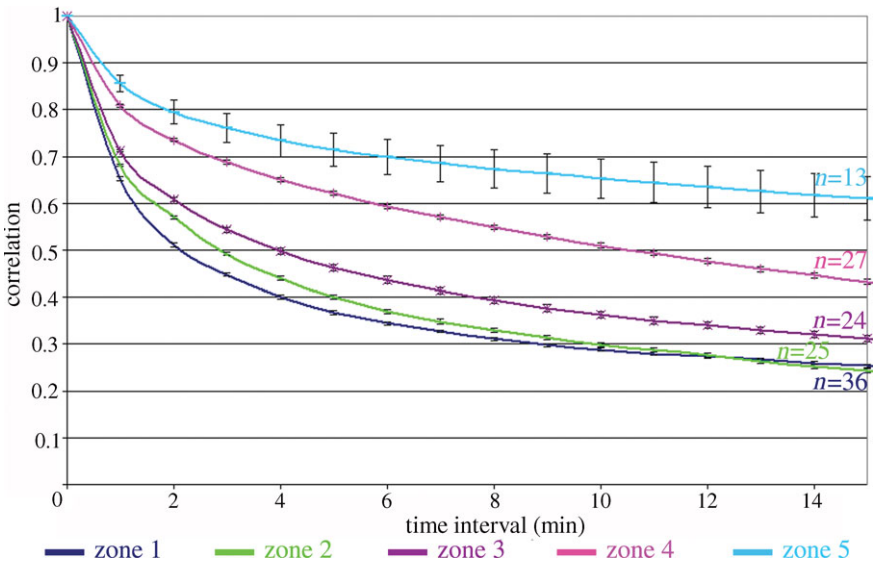

Figure 6. Correlation graph representing the stability of the sealing-zone rings on the five different topographical zones described in figure 3. The per cent averaged correlation of frames is plotted against the time interval between the different frames. The number of cells (n) is denoted for each graph. The stability of the sealing-zone rings increases as the surface becomes rougher. Error bars are standard errors.

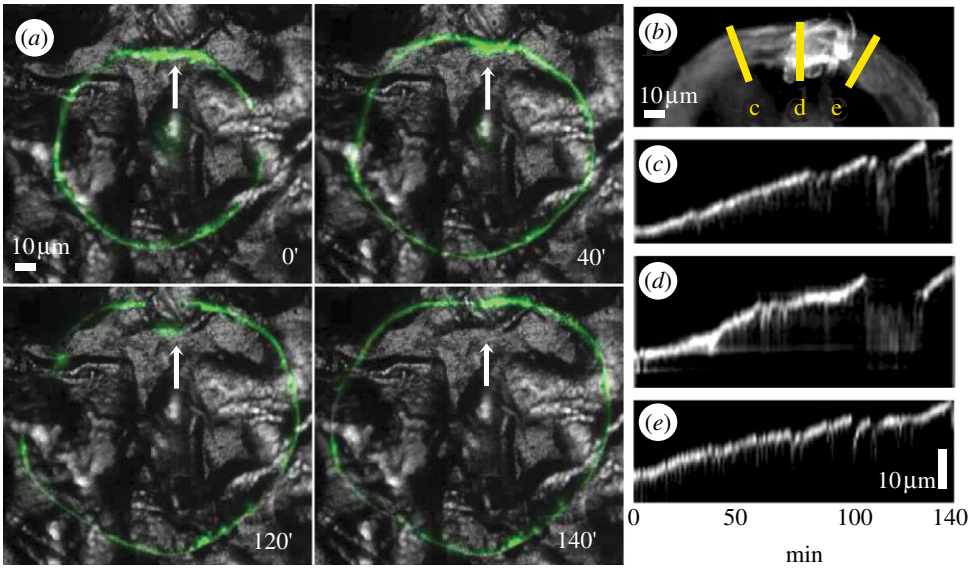

Figure 7. A sealing zone encountering an edge parallel to the sealing-zone tangent. (a) Frames from a live-cell imaging sequence. Note that along the edge, the sealing-zone movement is stalled but around the edge, the movement is continuous. (b) An overlay of the 140 min movie in (a). The lines represent the kymographs in (c–e). (c–e) Kymograph of three lines: in the place where the ring is stalled (d) and on the two flanking regions (c,e). Note that the movement is stalled relative to the sides, but then the ring eventually crosses the barrier and the movement is resumed. The kymograph abscissa represents the time evolution of the movement.

Live-cell monitoring of cultured osteoclasts indicates that sealing-zone expansion involves the assembly of new podosomes along the outer rim of the ring, and dissociation of internal podosomes [13]. In BHK-RSV cells, in which podosomes create expanding rings similar to the osteoclast sealing zone, paxillin phosphorylation has been shown to induce podosome disassembly at the inner rim of the ring, thus proving to be crucial to the process of ring expansion [33]. An attractive possibility is that the interconnecting F-actin filaments associated with the sealing zone apply pulling forces onto the podosomes associated with the outer circumference of the sealing zone. Similar to other integrin adhesions [34–40], these forces might enhance podosome assembly in these areas, and thus support ring expansion. The structural integrity of the ring depends on the fine balance between the formation and maturation of new podosomal rings and the outward extension rate. Typically, the formation of new podosomes lasts approximately 2 min (C. Luxenburg 2009, unpublished data), whereas the rate of ring expansion is irregular, depending on surface roughness and can be as fast as 2 µm min^{-1}. Ring expansion thus occurs within the same timescale as podosome formation, and may involve the formation of several podosomes per minute at any given location.

An inverse correlation between sealing-zone stability and integrity can be deduced from the same data. When the ring expands fast, as on a smooth surface, new

podosomes have insufficient time to assemble and interconnect to the existing sealing zone-associated podosomes, and therefore the sealing-zone ring is often fragmented. When the sealing-zone translocation is slower, as observed on rough surfaces, new podosomes have sufficient time to accumulate and interconnect and therefore the sealing zone is continuous.

What are the topographical features of the surface that affect sealing-zone formation, integrity and stability? To address this issue, one must understand the nature of the surfaces used in this study. The surfaces were prepared by replication of a metal sheet that was gradually polished after being sandblasted. During such a polishing process, which preferentially removes the short-wavelength components first, in parallel to total roughness (R_a) decrease, the slopes in the sample are less steep as the duration of polishing is longer. We suggest that the sealing-zone dynamics are regulated both by the magnitude of slopes in the sample and by the amount of nearly vertical 'ridges', each by different mechanisms.

Monitoring the local effect of topographical obstacles on sealing-zone structure and dynamics indicated that an edge up to several micrometres high, running perpendicular to the sealing-zone circumference, does not significantly alter the local ring-extension rate, while a barrier with similar dimensions, oriented parallel to the ring, locally blocks its expansion. When the surface is coated with sharp edges in all directions, at some point, the sealing-zone translocation will be arrested circumferentially by edges, leading to less circular and more stable sealing-zone rings, as was statistically observed. Naturally, when the barrier is larger than the ring diameter, the expansion of the sealing zone in that direction is completely arrested.

When the obstacle is significantly smaller than the ring diameter, those regions of the ring that do not directly encounter the barrier keep expanding, and consequently the sealing zone becomes convex. This process of local 'slowing down' of sealing-zone expansion is often overcome by cooperative processes, whereby advancing regions of the ring, flanking the arrested region, 'pull' the stalled ring over the physical obstacle. These observations indicate that 'outward-directed' radial forces drive sealing-zone dynamics and can have a long-range global effect, enabling stalled regions to overcome local topographical barriers. We have recently observed, however, that lack of surface adhesion constitutes an insurmountable barrier (F. Anderegg 2011, unpublished data). Thus, overcoming a topographical barrier still requires continuous adhesion to the surface.

Our previous observations on calcite [19] demonstrated that roughness in the sub-micrometre range promotes ring stability. Calcite, having only one stable face, possesses only very sharp edges and steps. The fact that sharp edges in the sub-micrometre range have a similar stabilizing effect over the sealing-zone stability as ridges with a height of several micrometres on the titanium gradients is explained by the decomposition of the total roughness (unfiltered; figure 3*d*) into components of different wavelength: this procedure shows that even though the total roughness is in the range of several micrometres, the height of the effective components lies in a range between a few hundreds of nanometres up to a maximum of 2.5 μm, as on calcite. Thus, knowledge of the unfiltered roughness value itself is insufficient for the prediction of ring stability.

Differences in sealing-zone dynamics were also observed between zones that possess no sharp edges. The regulation of ring dynamics can be explained by a complementary mechanism. As the podosomes are directly attached to the underlying surface, neighbouring podosomes can be anchored to the same plane or at different altitudes, depending on the topography of the surface to which they attach. The difference in altitude causes variations in the proximity of the podosome cores and, as a consequence, in the length and angle of the connecting fibres. Hence, the map of forces that the podosomes exert on one another is directly related to the underlying topography.

5. CONCLUSIONS

Bone degradation by osteoclasts depends on the effective sealing of the degradation lacuna, into which the osteoclast secretes acid and proteolytic enzymes. Thus, in order for resorption to be effective, the sealing zone must be coherent and stable for extended periods of time. The results illustrated here, together with those from our previous study [19], show that the latter requirements are met when the surfaces to which osteoclasts adhere are rough, ranging from hundreds of nanometres to micrometres, within the appropriate lateral wavelength scale, and contain microtopographic obstacles that slow down sealing-zone expansion. We further show that sealing-zone dynamics, while being locally regulated by surface roughness, can be globally mechanically integrated, most likely by the actin filaments that interconnect the constituting podosomes. We propose that the results presented in this study may be implemented in the design of novel implants, by controlling the implant topography, and thus improve osseointegration through direct effects on local bone resorption and global stimulation of bone remodelling.

We would like to acknowledge the Electron Microscopy Centre of ETH Zurich (EMEZ) for the use of their equipment. B.G. holds the Erwin Neter Professorial Chair in Cell and Tumor Biology, and L.A. the Dorothy and Patrick Gorman Chair of Biological Ultrastructure. This study was supported by a grant from the Israel Science Foundation (L.A.), the T3Net project of the EU-FP7 programme (B.G.) and an NIGMS grant from the Cell Migration Consortium (NIH grant U54GM64346) (B.G.).

REFERENCES

1 Roodman, G. D. 1996 Advances in bone biology: the osteoclast. *Endocr. Rev.* **17**, 308–332.
2 Engh, C. A., O'Connor, D., Jasty, M., McGovern, T. F., Bobyn, J. D. & Harris, W. H. 1992 Quantification of implant micromotion, strain shielding, and bone-resorption with porous-coated anatomic medullary locking femoral prostheses. *Clin. Orthop. Relat. Res.* **285**, 13–29.
3 Gilbert, J. L., Bloomfeld, R. S., Lautenschlager, E. P. & Wixson, R. L. 1992 A computer-based biomechanical

analysis of the 3-dimensional motion of cementless hip prostheses. *J. Biomech.* **25**, 329–340. (doi:10.1016/0021-9290(92)90252-V)
4 Vaananen, H. K. & Horton, M. 1995 The osteoclast clear zone is a specialized cell-extracellular matrix adhesion structure. *J. Cell Sci.* **108**, 2729–2732.
5 Luxenburg, C., Geblinger, D., Klein, E., Anderson, K., Hanein, D., Geiger, B. & Addadi, L. 2007 The architecture of the adhesive apparatus of cultured osteoclasts: from podosome formation to sealing zone assembly. *PLoS ONE* **2**, e179. (doi:10.1371/journal.pone.0000179)
6 Chellaiah, M., Kizer, N., Silva, M., Alvarez, U., Kwiatkowski, D. & Hruska, K. A. 2000 Gelsolin deficiency blocks podosome assembly and produces increased bone mass and strength. *J. Cell Biol.* **148**, 665–678. (doi:10.1083/jcb.148.4.665)
7 Calle, Y., Jones, G. E., Jagger, C., Fuller, K., Blundell, M. P., Chow, J., Chambers, T. & Thrasher, A. J. 2004 WASp deficiency in mice results in failure to form osteoclast sealing zones and defects in bone resorption. *Blood* **103**, 3552–3561. (doi:10.1182/blood-2003-04-1259)
8 Zambonin Zallone, A., Teti, A., Gaboli, M. & Marchisio, P. C. 1989 Beta 3 subunit of vitronectin receptor is present in osteoclast adhesion structures and not in other monocyte-macrophage derived cells. *Connect. Tissue Res.* **20**, 143–149. (doi:10.3109/03008208909023882)
9 Zambonin-Zallone, A., Teti, A., Grano, M., Rubinacci, A., Abbadini, M., Gaboli, M. & Marchisio, P. C. 1989 Immunocytochemical distribution of extracellular matrix receptors in human osteoclasts: a beta 3 integrin is colocalized with vinculin and talin in the podosomes of osteoclastoma giant cells. *Exp. Cell Res.* **182**, 645–652. (doi:10.1016/0014-4827(89)90266-8)
10 Pfaff, M. & Jurdic, P. 2001 Podosomes in osteoclast-like cells: structural analysis and cooperative roles of paxillin, proline-rich tyrosine kinase 2 (Pyk2) and integrin alpha-Vbeta3. *J. Cell Sci.* **114**, 2775–2786.
11 Luxenburg, C., Addadi, L. & Geiger, B. 2006 The molecular dynamics of osteoclast adhesions. *Eur. J. Cell Biol.* **85**, 203–211. (doi:10.1016/j.ejcb.2005.11.002)
12 Lakkakorpi, P. T. & Vaananen, H. K. 1996 Cytoskeletal changes in osteoclasts during the resorption cycle. *Microsc. Res. Tech.* **33**, 171–181. (doi:10.1002/(SICI)1097-0029(19960201)33:2<171::AID-JEMT7>3.0.CO;2-W)
13 Destaing, O., Saltel, F., Geminard, J. C., Jurdic, P. & Bard, F. 2003 Podosomes display actin turnover and dynamic self-organization in osteoclasts expressing actin-green fluorescent protein. *Mol. Biol. Cell* **14**, 407–416. (doi:10.1091/mbc.E02-07-0389)
14 Saltel, F., Destaing, O., Bard, F., Eichert, D. & Jurdic, P. 2004 Apatite-mediated actin dynamics in resorbing osteoclasts. *Mol. Biol. Cell* **15**, 5231–5241. (doi:10.1091/mbc.E04-06-0522)
15 Redey, S. A., Razzouk, S., Rey, C., Bernache-Assollant, D., Leroy, G., Nardin, M. & Cournot, G. 1999 Osteoclast adhesion and activity on synthetic hydroxyapatite, carbonated hydroxyapatite, and natural calcium carbonate: relationship to surface energies. *J. Biomed. Mater. Res.* **45**, 140–147. (doi:10.1002/(SICI)1097-4636(199905)45:2<140::AID-JBM9>3.0.CO;2-I)
16 Monchau, F., Lefevre, A., Descamps, M., Belquin-myrdycz, A., Laffargue, P. & Hildebrand, H. F. 2002 *In vitro* studies of human and rat osteoclast activity on hydroxyapatite, beta-tricalcium phosphate, calcium carbonate. *Biomol. Eng.* **19**, 143–152. (doi:10.1016/S1389-0344(02)00023-0)
17 Nakamura, I., Takahashi, N., Sasaki, T., Jimi, E., Kurokawa, T. & Suda, T. 1996 Chemical and physical properties of the extracellular matrix are required for the actin ring formation in osteoclasts. *J. Bone Miner. Res.* **11**, 1873–1879. (doi:10.1002/jbmr.5650111207)
18 Geblinger, D., Geiger, B. & Addadi, L. 2009 Surface-induced regulation of podosome organization and dynamics in cultured osteoclasts. *Chembiochem* **10**, 158–165. (doi:10.1002/cbic.200800549)
19 Geblinger, D., Addadi, L. & Geiger, B. 2010 Nano-topography sensing by osteoclasts. *J. Cell Sci.* **123**, 1503–1510. (doi:10.1242/jcs.060954)
20 Baharloo, B., Textor, M. & Brunette, D. M. 2005 Substratum roughness alters the growth, area, and focal adhesions of epithelial cells, and their proximity to titanium surfaces. *J. Biomed. Mater. Res. A* **74**, 12–22.
21 Ball, M., Grant, D. M., Lo, W. J. & Scotchford, C. A. 2008 The effect of different surface morphology and roughness on osteoblast-like cells. *J. Biomed. Mater. Res. A* **86**, 637–647.
22 Curtis, A. & Wilkinson, C. 1997 Topographical control of cells. *Biomaterials* **18**, 1573–1583. (doi:10.1016/S0142-9612(97)00144-0)
23 Deligianni, D. D., Katsala, N. D., Koutsoukos, P. G. & Missirlis, Y. F. 2001 Effect of surface roughness of hydroxyapatite on human bone marrow cell adhesion, proliferation, differentiation and detachment strength. *Biomaterials* **22**, 87–96. (doi:10.1016/S0142-9612(00)00174-5)
24 Huang, H. H., Ho, C. T., Lee, T. H., Lee, T. L., Liao, K. K. & Chen, F. L. 2004 Effect of surface roughness of ground titanium on initial cell adhesion. *Biomol. Eng.* **21**, 93–97. (doi:10.1016/j.bioeng.2004.05.001)
25 Kunzler, T. P., Drobek, T., Schuler, M. & Spencer, N. D. 2007 Systematic study of osteoblast and fibroblast response to roughness by means of surface-morphology gradients. *Biomaterials* **28**, 2175–2182. (doi:10.1016/j.biomaterials.2007.01.019)
26 Kunzler, T. P., Huwiler, C., Drobek, T., Voros, J. & Spencer, N. D. 2007 Systematic study of osteoblast response to nanotopography by means of nanoparticle-density gradients. *Biomaterials* **28**, 5000–5006. (doi:10.1016/j.biomaterials.2007.08.009)
27 Makihira, S., Mine, Y., Kosaka, E. & Nikawa, H. 2007 Titanium surface roughness accelerates RANKL-dependent differentiation in the osteoclast precursor cell line, RAW264.7. *Dent. Mater. J.* **26**, 739–745. (doi:10.4012/dmj.26.739)
28 Marchisio, M., Di Carmine, M., Pagone, R., Piattelli, A. & Miscia, S. 2005 Implant surface roughness influences osteoclast proliferation and differentiation. *J. Biomed. Mater. Res. B Appl. Biomater.* **75**, 251–256.
29 Price, R. L., Ellison, K., Haberstroh, K. M. & Webster, T. J. 2004 Nanometer surface roughness increases select osteoblast adhesion on carbon nanofiber compacts. *J. Biomed. Mater. Res. A* **70**, 129–138. (doi:10.1002/jbm.a.30073)
30 Luxenburg, C., Parsons, J. T., Addadi, L. & Geiger, B. 2006 Involvement of the Src-cortactin pathway in podosome formation and turnover during polarization of cultured osteoclasts. *J. Cell Sci.* **119**, 4878–4888. (doi:10.1242/jcs.03271)
31 Wieland, M., Hanggi, P., Hotz, W., Textor, M., Keller, B. A. & Spencer, N. D. 2000 Wavelength-dependent measurement and evaluation of surface topographies: application of a new concept of window roughness and surface transfer function. *Wear* **237**, 231–252. (doi:10.1016/S0043-1648(99)00347-6)
32 Jurdic, P., Saltel, F., Chabadel, A. & Destaing, O. 2006 Podosome and sealing zone: specificity of the osteoclast model. *Eur. J. Cell Biol.* **85**, 195–202. (doi:10.1016/j.ejcb.2005.09.008)

33 Badowski, C., Pawlak, G., Grichine, A., Chabadel, A., Oddou, C., Jurdic, P., Pfaff, M., Albiges-Rizo, C. & Block, M. R. 2008 Paxillin phosphorylation controls invadopodia/podosomes spatiotemporal organization. *Mol. Biol. Cell* **19**, 633–645. (doi:10.1091/mbc.E06-01-0088)

34 Geiger, B. & Bershadsky, A. 2001 Assembly and mechanosensory function of focal contacts. *Curr. Opin. Cell Biol.* **13**, 584–592. (doi:10.1016/S0955-0674(00)00255-6)

35 Bershadsky, A., Kozlov, M. & Geiger, B. 2006 Adhesion-mediated mechanosensitivity: a time to experiment, and a time to theorize. *Curr. Opin. Cell Biol.* **18**, 472–481. (doi:10.1016/j.ceb.2006.08.012)

36 Geiger, B., Spatz, J. P. & Bershadsky, A. D. 2009 Environmental sensing through focal adhesions. *Nat. Rev. Mol. Cell Biol.* **10**, 21–33. (doi:10.1038/nrm2593)

37 Bershadsky, A. D. *et al.* 2006 Assembly and mechanosensory function of focal adhesions: experiments and models. *Eur. J. Cell Biol.* **85**, 165–173. (doi:10.1016/j.ejcb.2005.11.001)

38 Riveline, D., Zamir, E., Balaban, N. Q., Schwarz, U. S., Ishizaki, T., Narumiya, S., Kam, Z., Geiger, B. & Bershadsky, A. D. 2001 Focal contacts as mechanosensors: externally applied local mechanical force induces growth of focal contacts by an mDia1-dependent and ROCK-independent mechanism. *J. Cell Biol.* **153**, 1175–1186. (doi:10.1083/jcb.153.6.1175)

39 Balaban, N. Q. *et al.* 2001 Force and focal adhesion assembly: a close relationship studied using elastic micropatterned substrates. *Nat. Cell Biol.* **3**, 466–472. (doi:10.1038/35074532)

40 Bershadsky, A. D., Balaban, N. Q. & Geiger, B. 2003 Adhesion-dependent cell mechanosensitivity. *Annu. Rev. Cell Dev. Biol.* **19**, 677–695. (doi:10.1146/annurev.cellbio.19.111301.153011)